Identifying Quantum Many-Body Integrability and Chaos Using Eigenstate Trace Distances

Reyhaneh Khasseh,[1] Jiaju Zhang,[2] Markus Heyl,[1] and M. A. Rajabpour[3]
[1]Theoretical Physics III, Center for Electronic Correlations and Magnetism, Institute of Physics, University of Augsburg, D-86135 Augsburg, Germany
[2]Center for Joint Quantum Studies and Department of Physics, School of Science, Tianjin University, 135 Yaguan Road, Tianjin 300350, China
[3]Instituto de Fisica, Universidade Federal Fluminense, Av. Gal. Milton Tavares de Souza s/n, Gragoatá, 24210-346 Niterói, Rio de Janeiro, Brazil

(Received 15 February 2023; accepted 29 September 2023; published 22 November 2023)

While the concepts of quantum many-body integrability and chaos are of fundamental importance for the understanding of quantum matter, their precise definition has so far remained an open question. In this Letter, we introduce an alternative indicator for quantum many-body integrability and chaos, which is based on the statistics of eigenstates by means of nearest-neighbor subsystem trace distances. We show that this provides us with a faithful classification through extensive numerical simulations for a large variety of paradigmatic model systems including random matrix theories, free fermions, Bethe-ansatz solvable systems, and models of many-body localization. While existing indicators, such as those obtained from level-spacing statistics, have already been utilized with great success, they also face limitations. This concerns, for instance, the quantum many-body kicked top, which is exactly solvable but classified as chaotic in certain regimes based on the level-spacing statistics, while our introduced indicator signals the expected quantum many-body integrability. We discuss the universal behaviors we observe for the nearest-neighbor trace distances and point out that our indicator might be useful also in other contexts such as for the many-body localization transition.

DOI: 10.1103/PhysRevLett.131.216701

Quantum chaos and integrability have been a major focus of research for decades due to their key relevance for the foundations of statistical physics and fundamental concepts such as thermalization. In classical physics, chaos manifests as a divergence of initially close-by phase-space trajectories. Integrability as a counterpart of chaos is defined by the existence of a maximal number of Poisson-commuting invariants [1,2]. However, establishing a precise measure of quantum chaos and integrability in the quantum many-body regime has remained an outstanding challenge [3]. The most widely used indicator is based on level spacing statistics [4,5]. However, it predicts chaotic behavior for some systems, which are expected to be considered integrable in the many-body sense [6,7].

In this Letter, we introduce an alternative indicator of quantum integrability and many-body quantum chaos based on the eigenstate properties instead of the spectrum. We show that our indicator correctly classifies a wide range of systems as quantum integrable, including Bethe-ansatz solvable models, quantum spin chains in a fully many-body localized (MBL) regime, and quadratic fermionic systems. It is a central result of this Letter that our indicator detects quantum integrability also in cases where the level spacing fails, such as the quantum many-body kicked-top model. Our indicator is based on subsystem trace distances between nearest-neighboring Hamiltonian eigenstates, which provides a bound on the smoothness of operator expectation values as a function of energy and, therefore, a natural connection to the eigenstate thermalization hypothesis (ETH). This measure is much more robust to the symmetries of the systems as compared to the level spacing statistics. This can be useful when the symmetries of a model are not fully understood.

To investigate whether a general quantum Hamiltonian exhibits chaos or integrability, we evaluate the trace norm distance between two reduced density matrices defined as

$$D_n^A = \frac{1}{2}||\rho_{n+1}^A - \rho_n^A||_1. \tag{1}$$

Here, $\rho_n^A = \mathrm{Tr}_{\bar{A}}\rho_n$ denotes the reduced density matrix of a subsystem A and $\rho_n = |\psi_n\rangle\langle\psi_n|$ the density matrix of an eigenstate $|\psi_n\rangle$ of a given Hamiltonian. We order the eigenstates $|\psi_n\rangle$ with respect to their eigenvalues ϵ_n in ascending order, i.e., $\epsilon_{n+1} > \epsilon_n$. While distances between density matrices can be defined in various ways [8–10], the definition in Eq. (1) turns out to be practically suitable, as we will discuss in the remainder of this Letter. In particular, it has been found that D_n^A provides a general

upper bound on the smoothness of operator expectation values as a function of energy [10,11]:

$$|\Delta\mathcal{O}_n| = |\mathrm{Tr}(\rho^A_{n+1} - \rho^A_n)\mathcal{O}| \leq 2sD^A_n. \tag{2}$$

Here, $\Delta\mathcal{O}_n = \langle\psi_{n+1}|\mathcal{O}|\psi_{n+1}\rangle - \langle\psi_n|\mathcal{O}|\psi_n\rangle$ denotes the difference of operator expectation values in neighboring eigenstates with $\mathcal{O}$ an operator defined in subsystem A and s is the largest singular value of the operator $\mathcal{O}$ [10]. The expectation values of local observables for various Hamiltonian eigenstates may fluctuate between neighboring eigenstates and conform to thermal predictions if the ETH is valid. This distinction can be used to differentiate between integrable and chaotic models. The ETH, which pertains to chaotic Hamiltonians, stipulates that the diagonal matrix elements of observables within Hamiltonian eigenstates exhibit a smooth energy dependence and a narrow distribution. Conversely, in the integrable regime, the expectation values across the spectrum tend to fluctuate significantly, as previously demonstrated in various research studies (see Refs. [12,13] for a review). We propose to use the eigenstate trace distances measure in Eq. (1), which expands upon the definition of the ETH based on subsystem trace distances in Ref. [14] by providing quantitative criteria for quantum many-body chaos and integrability.

In the following, we will introduce the microscopic chaotic and integrable models we use to illustrate our findings.

Many-body quantum chaotic systems.—Let us start with the analysis of many-body quantum chaotic systems. In this context, we will use for our analysis the paradigmatic quantum Ising chain with both transverse and longitudinal fields

$$H_{\mathrm{Ising}} = \sum_{l=1}^{L}(J\sigma^z_l\sigma^z_{l+1} + h_z\sigma^z_l + h_x\sigma^x_l), \tag{3}$$

where $\sigma^\alpha_l(\alpha = x, y, z)$ denote the Pauli spin operators at site l, J is the coupling constant, and $h_\beta(\beta = x, z)$ represent the strengths of the two magnetic fields. In what follows, we will set the interaction $J = 1$. We assume periodic boundary conditions (PBCs), i.e., $\sigma^\alpha_{L+1} = \sigma^\alpha_1(\alpha = x, y, z)$, which implies translational invariance. This symmetry enables us to partition the Hamiltonian into different sectors with a conserved momentum of $K = 2\pi j/L$, where $j = 0, \ldots, L-1$. Each sector can be independently diagonalized, reducing the computational complexity. It is worth noting that the main features of the statistics of D^A_n are identical for single symmetry sectors or for the full spectrum. We, therefore, focus on a single sector $K = 2\pi/L$ without loss of generality. Let us mention, however, that the $K = 0, \pi$ sectors provide an exception due to the presence of further symmetries. Examples of different symmetry blocks and comparisons with results from the full spectrum can be found in the Supplemental Material [15]. In the following, it will be suitable to analyze D^A_n as a function of $x = L_A/L$, so that we introduce the following notation:

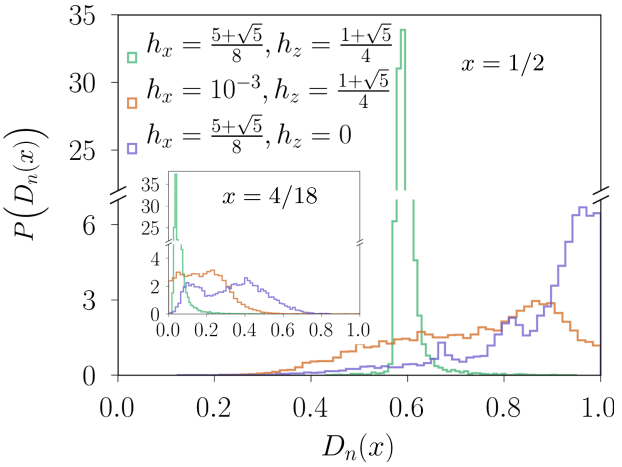

FIG. 1. Ising model: Distribution $P[D_n(x)]$ of trace distances $D_n(x)$ for nearest-neighbor eigenstates with $x = L_A/L$, the ratio between subsystem size L_A and system size $L = 18$. The main plot shows data for $P[D_n(x)]$ at different magnetic field strengths for $L_A = L/2$ and the inset for $L_A = 4$, focusing on one symmetry sector: $K = 2\pi/L$.

$$D_n(x) = \frac{1}{2}||\rho_{n+1}(x) - \rho_n(x)||_1, \quad x = L_A/L, \tag{4}$$

in addition to Eq. (1).

The Ising chain, which is described in Eq. (3), is known to exhibit chaotic behavior as long as J and $h_{x,z}$ are nonzero [24]. In Fig. 1, we show the qualitatively different behaviors of the distribution of $D_n(x)$ in the integrable and quantum chaotic regimes for a system of size $L = 18$ and for $x = 1/2, 2/9$, respectively. The distribution is narrow and strongly peaked for the quantum chaotic case, and we find that the width of the distribution is exponentially suppressed with the system size in this limit, see Fig. S1(a) in the Supplemental Material [15]. This result is consistent with RMT, where the distribution is Gaussian, with a vanishing standard deviation by increasing the size of the system, see Figs. S1(a) and S1(b) in the Supplemental Material [15]. Turning off either the longitudinal or transverse field results in an integrable model with a much broader distribution, as shown in Fig. 1.

In what follows, we will consider as a detector of quantum many-body chaos and integrability the mean value $\langle D_n(x)\rangle$ taken over all eigenstates in a single momentum sector. In the chaotic regime, we see that $\langle D_n(x)\rangle$ decays upon increasing system size L as long as $x < 1/2$, see Figs. 2(a) and 2(b) for the chaotic Ising model and the Gaussian orthogonal ensemble (GOE) from random matrix theory (RMT). As we show analytically in

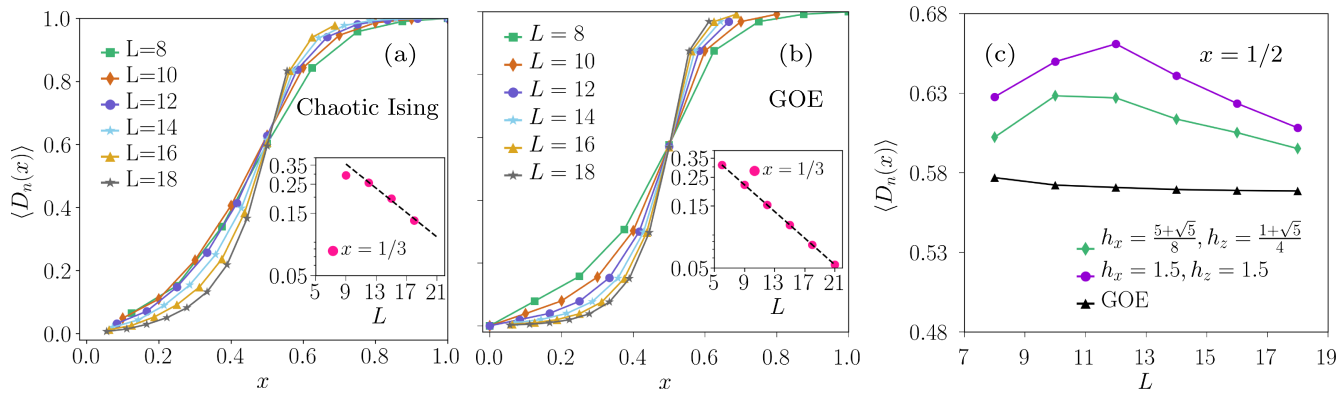

FIG. 2. Quantum many-body chaotic models: (a) average $\langle D_n(x)\rangle$ for the Ising chain at $h_z = (1+\sqrt{5})/4$ and $h_x = (5+\sqrt{5})/8$ in the symmetry sector with $K = 2\pi/L$. (b) $\langle D_n(x)\rangle$ for RMT from the Gaussian orthogonal ensemble (GOE) taken over 4000 random eigenstates. The inset shows the exponential decay of $\langle D_n(x)\rangle$ with system size L for the case of $x = 1/3$. In panel (c), we compare the system-size dependence of $\langle D_n(x = 1/2)\rangle$ in the quantum many-body chaotic Ising model with RMT.

Sec. II of the Supplemental Material [15], the ETH predicts the following behavior:

$$\langle D_n(x)\rangle = C\Delta, \tag{5}$$

where $\Delta = \langle \epsilon_{n+1} - \epsilon_n\rangle$ denotes the mean level spacing and C a prefactor, which will be discussed in more detail below. Since Δ decays exponentially with system size L for large systems, we find that this is consequently also the case for $D_n(x)$. This holds as long as the ETH applies to the considered model system, requiring that the system size L is sufficiently large. From the insets of Figs. 2(a) and 2(b) at a fixed $x = 1/3$ we further see that the GOE exhibits compelling evidence for an exponential decay, as predicted by Eq. (5). For the chaotic Ising model the behavior is less pronounced due to limitations from the accessible system sizes, but also consistent with the predicted exponential decay.

As we further show analytically in Sec. II of the Supplemental Material [15], we can additionally bound the proportionality constant C. For that purpose we have to assume in addition to the ETH that the subsystem density matrix itself can be approximated well by a canonical density matrix. This requires us to take the usual limits of statistical mechanics requiring the subsystem to be very large, but still much smaller than the total system. In this regime we find that $C \leq 1/\Delta E$ with $\Delta E = \sqrt{\langle H^2\rangle - \langle H\rangle^2}$ the total energy fluctuations yielding a system-size dependence proportional to $1/\sqrt{L}$. Notice, however, that for the system sizes considered in Fig. 2, the aforementioned requirements are not yet met. Thus, the derived bound on C should be viewed more as an asymptotic behavior.

In Fig. 2, we show numerical data of $\langle D_n(x)\rangle$ for many-body quantum chaotic models. We find that $x = 1/2$ is a fixed point, and the behavior of $\langle D_n(x)\rangle$ is different for values of x less than and greater than $1/2$. For $x < 1/2$, $\langle D_n(x)\rangle$ decays upon increasing L, ultimately tending towards zero as L approaches infinity. These results align with the recent study [25], which carried out analytical assessments of $\langle D_n(x)\rangle$ for random states and has delved into its application in the Ising model for small sizes. For $x > 1/2$, $\langle D_n(x)\rangle$ tends towards 1 by increasing system size. To emphasize the consistency of the results of the chaotic Ising chain with RMT, we study in more detail $\langle D_n(1/2)\rangle$ in Fig. 2(c). One can see that for large system sizes $\langle D_n(1/2)\rangle$ in the chaotic Ising model approaches the saturation value of RMT. More details about RMT are discussed in Sec. I of the Supplemental Material [15].

Integrable systems.—After discussing the behavior of $\langle D_n(x)\rangle$ for quantum many-body chaotic systems, we now move to the case of integrable models. In particular, we first study the transverse-field Ising chain at $h_z = 0$ in Eq. (3). Since the model is integrable in this regime, we expect the results to be significantly different from those predicted by RMT. We show the markedly different behavior in Fig. 3(a) where we provide numerical data for $\langle D_n(x)\rangle$ for different system sizes. First of all, we cannot identify a fixed point anymore. Upon increasing system size, we find that $\langle D_n(x)\rangle$ appears to converge to a single nonzero curve that does not match the prediction of the ETH in Eq. (5). Instead, the numerical data seem to approach a linear function $\langle D_n(x)\rangle \sim ax$ upon increasing system size with a slope $a \approx 2$. The linear slope remains roughly unchanged when considering other symmetry blocks except those with $K = 0, \pi$, which have $a \approx 1$ [26]. This is discussed further in Sec. III of the Supplemental Material [15].

In order to gain some analytical insights into this linear behavior, we have also studied the XY chain, which can be solved exactly through a mapping to a free fermion Hamiltonian using the Jordan-Wigner transformation [27–29]. The subsystem trace distance between two eigenstates can be obtained by explicit construction of the RDMs [30–32]. We find evidence that $\langle D_n(x)\rangle \propto x$ in the large L limit, especially in the range $x \in (0.1, 0.4)$, see Sec. IV of the Supplemental Material [15].

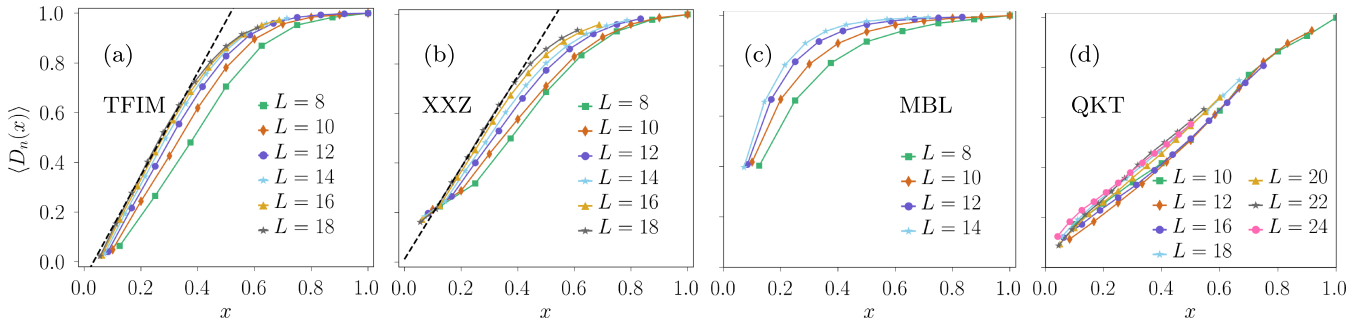

FIG. 3. Quantum many-body integrable models: (a) $\langle D_n(x)\rangle$ as a function of $x = L_A/L$ for the transverse field Ising model (TFIM) with $h_x = (5+\sqrt{5})/8$ and $h_z = 0$. The dashed line marks the linear ax with $a \approx 2$. (b) $\langle D_n(x)\rangle$ for the Bethe-ansatz integrable XXZ chain with $\Delta = 2$. Again, we have included a dashed line indicating linear behavior ax with $a \approx 2$. (c) XXZ model with $\Delta = 2$ and strong disorder $h = 10$ in the MBL regime. (d) Quantum kicked top (QKT) model at $\kappa = 7$ and $\tau = 1$. In (a), (b), and (c) we focus on the symmetry block with $K = 2\pi/L$, and in (d) the $S = L/2$ sector.

In the following, we will now explore to what extent this observed behavior for the Ising chain generalizes also to other models, including the Bethe-ansatz integrable homogeneous XXZ chain, the XXZ model with a random field in the MBL regime, and the quantum many-body kicked top.

The Hamiltonian of the XXZ model is given by

$$H_{XXZ} = \sum_{l=1}^{L} (\sigma_l^x \sigma_{l+1}^x + \sigma_l^y \sigma_{l+1}^y + \Delta \sigma_l^z \sigma_{l+1}^z + h_z^l \sigma_l^z), \quad (6)$$

where Δ denotes the anisotropy parameter. We will consider two cases for the magnetic field h_z^l. On the one hand, we take $h_z^l = h_z$ uniform, where Eq. (6) yields the Bethe-ansatz integrable XXZ model. On the other hand, we will consider $h_z^l \in [-h, h]$ a random variable drawn from the uniform distribution, which gives a paradigmatic model for MBL [33,34].

In Fig. 3(b), we show numerical data of $\langle D_n(x)\rangle$ for the Bethe-ansatz integrable limit. We observe a similar behavior as compared to the integrable Ising chain. Again, $\langle D_n(x)\rangle$ doesn't align with the ETH prediction of Eq. (5), but rather approaches a linear behavior as a function of x with a slope $a \approx 2$ as in the case of the Ising chain.

For the case of strong random fields, the XXZ model enters an MBL phase [33,34], violating the ETH. Systems in the fully MBL regime are expected to show an emergent form of integrability caused by the presence of an extensive number of emergent local conservation laws. The numerical results for the MBL case, see Fig. 3(c), again don't follow the ETH prediction in Eq. (5) so that our indicator correctly classifies such MBL systems as integrable. However, differently from the other integrable systems, we don't observe a linear behavior of $\langle D_n(x)\rangle$ as a function of x. $\langle D_n(x)\rangle$ rather appears to approach $\langle D_n(x)\rangle \to 1$ upon increasing system size.

Finally, we investigate a many-body Floquet system whose dynamics is captured by the following Hamiltonian [35]

$$H = h_x \sum_{l=1}^{L} \sigma_l^x + \frac{\kappa}{L} \sum_{l,m=1}^{L} \sigma_l^z \sigma_m^z \sum_{n=-\infty}^{+\infty} \delta(t - n\tau), \quad (7)$$

where the transverse field and kick strength are represented by h_x and κ, respectively, and the kicks have a period of τ. This is the so-called quantum kicked top (QKT). In this model, the collective spin operator $S^2 = S_x^2 + S_y^2 + S_z^2$, with $S_\alpha = 1/2 \sum_i \sigma_i^\alpha$ where $\alpha = x, y, z$, is conserved. As a result, the Hilbert space of the system can be divided into subspaces with fixed total spin, in which the dynamics are equivalent to that of a single kicked top with the corresponding angular momentum S [36–38]. We analyze this explicitly time-dependent model using Floquet theory by means of the eigenstates of the Floquet operator $U_F = \exp(-i\kappa S_z^2/L)\exp(-ih_x\tau S_x)$, i.e., the time-evolution operator U_F over one period τ. As the analog of the eigenenergies we consider the quasienergies of the corresponding Floquet operator $H_F = -i\ln(U_F)$. In what follows, we perform the statistics for the largest Hilbert space subspace with $S = L/2$.

The key consequence of the aforementioned conservation law is that the largest subspace in Hilbert space is linear in system size L. Therefore, the exact solution can be obtained with an effort depending only polynomially on system size. As a consequence, we consider this model to be quantum many-body integrable. Let us directly emphasize, however, that this statement is not in contradiction to the well-known result that the kicked top is considered a paradigmatic quantum chaotic model in the single-particle sense. In particular, it has been shown that the level spacing statistics of individual blocks in Hilbert space can display GOE behavior whenever the parameter κ exceeds a critical value κ_c [36,39,40]. Such GOE behavior is a standard indicator of quantum chaos.

In Fig. 3(d) we show the results of $\langle D_n(x)\rangle$ for the QKT with $\kappa = 7$. One can clearly observe that $\langle D_n(x)\rangle$ doesn't follow the ETH prediction in Eq. (5) of an exponentially decaying $\langle D_n(x)\rangle$ with system size. We rather find that

$\langle D_n(x)\rangle$ behaves similar to the conventional integrable models such as the Ising chain or the XXZ model. Upon increasing system size, $\langle D_n(x)\rangle$ appears to approach a linear behavior upon increasing L. As a consequence, our indicator predicts the many-body quantum integrability of the QKT for $\kappa = 7$. It is noteworthy that, for small values of the parameter κ, the behavior of the observable $D_n(x)$ is unexpectedly consistent with that of a MBL system. Additional illustrations of this can be found in Sec. V of the Supplemental Material [15].

Conclusions.—In this Letter, we have presented an alternative indicator for quantum many-body integrability and chaos through trace distances of nearest-neighboring eigenstates, unlike traditional level spacing statistics focusing on Hamiltonian eigenvalues. In recent years many indicators based on local observables related to the reduced density matrix of small subsystems have been introduced. However, according to our analysis in Sec. VI of the Supplemental Material [15], examining the corresponding density matrix of larger subsystems (i.e., $x > 0$) proves more fruitful in discerning many-body integrable systems from chaotic regimes.

Trace distances also provide bounds on eigenstate-to-eigenstate fluctuations of some nonlocal quantities, such as the entanglement entropy and Rényi entropy [41–43], which have been used as alternative indicators for chaos, integrability, and MBL in quantum systems [44–46]. Let us point out, however, that by utilizing the entanglement entropy, say, as an indicator, it is essential to have analytical access to a reference, which is typically the Page value. While this allows us to study many-body quantum chaos at infinite temperature for bounded Hamiltonians, the indicator based on trace distances in our Letter exhibits a broader range of applicability as it can be also applied in an energy-resolved fashion, in principle, and also for unbounded Hamiltonians including bosonic systems.

For the future, it would be important to develop a deeper analytical understanding of our indicator $\langle D_n(x)\rangle$ in the quantum many-body integrable regimes, which so far has been mostly based on numerical results. A particularly interesting point might be to address the seemingly universal linear behavior of $\langle D_n(x)\rangle$ for certain integrable models and why certain other models, such as MBL systems, apparently behave differently. While we have covered a broad range of physical systems, extending our indicator's applicability to larger class of models is important. For instance, it would be interesting to apply the indicator to interacting systems with disorder, where recent developments have raised fundamental questions on the MBL phase and the MBL transition [47–50].

We acknowledge valuable discussions with A. Russomanno. This project has received funding from the European Research Council (ERC) under the European Union's Horizon 2020 research and innovation program (Grant Agreement No. 853443). M. A. R. thanks CNPq for partial support. J. Z. is thankful for support from the National Natural Science Foundation of China (NSFC) Grant No. 12205217.

[1] M. C. Gutzwiller, *Chaos in Classical and Quantum Mechanics* (Springer, New York, 2013), Vol. 1.
[2] O. Babelon, D. Bernard, and M. Talon, *Introduction to Classical Integrable Systems* (Cambridge University Press, Cambridge, England, 2003).
[3] J. S. Caux and J. Mossel, Remarks on the notion of quantum integrability, J. Stat. Mech. (2011) P02023.
[4] M. V. Berry and M. Tabor, Level clustering in the regular spectrum, Proc. R. Soc. A **356**, 375 (1977).
[5] O. Bohigas, M. J. Giannoni, and C. Schmit, Characterization of chaotic quantum spectra and universality of level fluctuation laws, Phys. Rev. Lett. **52**, 1 (1984).
[6] F. Finkel and A. González-López, Global properties of the spectrum of the Haldane-Shastry spin chain, Phys. Rev. B **72**, 174411 (2005).
[7] L. M. Sieberer, T. Olsacher, A. Elben, M. Heyl, P. Hauke, F. Haake, and P. Zoller, Digital quantum simulation, Trotter errors, and quantum chaos of the kicked top, npj Quantum Inf. **5**, 1 (2019).
[8] V. V. Dodonov, O. V. Man'Ko, V. I. Man'Ko, and A. Wünsche, Hilbert-Schmidt distance and non-classicality of states in quantum optics, J. Mod. Opt. **47**, 633 (2000).
[9] A. Gilchrist, N. K. Langford, and M. A. Nielsen, Distance measures to compare real and ideal quantum processes, Phys. Rev. A **71**, 062310 (2005).
[10] M. A. Nielsen and I. L. Chuang, *Quantum Computation and Quantum Information* (Cambridge University Press, Cambridge, England, 2009), ISBN: 9781107002173.
[11] J. Zhang, P. Calabrese, M. Dalmonte, and M. A. Rajabpour, Lattice Bisognano-Wichmann modular Hamiltonian in critical quantum spin chains, SciPost Phys. Core **2**, 007 (2020).
[12] M. Rigol, V. Dunjko, and M. Olshanii, Thermalization and its mechanism for generic isolated quantum systems, Nature (London) **452**, 854 (2008).
[13] J. M. Deutsch, Eigenstate thermalization hypothesis, Rep. Prog. Phys. **81**, 082001 (2018).
[14] A. Dymarsky, N. Lashkari, and H. Liu, Subsystem eigenstate thermalization hypothesis, Phys. Rev. E **97**, 012140 (2018).
[15] See Supplemental Material at http://link.aps.org/supplemental/10.1103/PhysRevLett.131.216701 for the detailed calculations of random matrix theory, analytical calculations using eigenstate thermalization hypothesis, robustness of trace distance measure to Hamiltonian symmetries, which includes Refs. [16–23].
[16] T. Guhr, A. Müller-Groeling, and H. A. Weidenmüller, Random-matrix theories in quantum physics: Common concepts, Phys. Rep. **299**, 189 (1998).
[17] P. J. Forrester, N. C. Snaith, and J. J. M. Verbaarschot, Developments in random matrix theory, J. Phys. A **36**, R1 (2003).

[18] G. Livan, M. Novaes, and P. Vivo, Introduction to random matrices theory and practice, Monograph Award **63**, 54–57 (2018).
[19] Y. Y. Atas, E. Bogomolny, O. Giraud, and G. Roux, Distribution of the ratio of consecutive level spacings in random matrix ensembles, Phys. Rev. Lett. **110**, 084101 (2018).
[20] J. A. Miszczak, Generating and using truly random quantum states in Mathematica, Comput. Phys. Commun. **183**, 118 (2012).
[21] J. R. Garrison and T. Grover, Does a single eigenstate encode the full Hamiltonian?, Phys. Rev. X **8**, 021026 (2018).
[22] A. Dymarsky, N. Lashkari, and H. Liu, Subsystem eigenstate thermalization hypothesis, Phys. Rev. E **97**, 012140 (2018).
[23] T. LeBlond, K. Mallayya, L. Vidmar, and M. Rigol, Entanglement and matrix elements of observables in interacting integrable systems, Phys. Rev. E **100**, 062134 (2019).
[24] H. Kim and D. A. Huse, Ballistic spreading of entanglement in a diffusive nonintegrable system, Phys. Rev. Lett. **111**, 127205 (2013).
[25] J. T. de Miranda and T. Micklitz, Subsystem trace-distances of two random states, J. Phys. A **56**, 175301 (2023).
[26] We note that due to the large number of degeneracies in these sectors there is an ambiguity in ordering the states, which leads to different slops depending on the method that one uses, see the Supplemental Material [15].
[27] E. Lieb, T. Schultz, and D. Mattis, Two soluble models of an antiferromagnetic chain, Ann. Phys. (N.Y.) **16**, 407 (1961).
[28] S. Katsura, Statistical mechanics of the anisotropic linear Heisenberg model, Phys. Rev. **127**, 1508 (1962).
[29] P. Pfeuty, The one-dimensional Ising model with a transverse field, Ann. Phys. (N.Y.) **57**, 79 (1970).
[30] J. Zhang, P. Ruggiero, and P. Calabrese, Subsystem trace distance in quantum field theory, Phys. Rev. Lett. **122**, 141602 (2019).
[31] J. Zhang, P. Ruggiero, and P. Calabrese, Subsystem trace distance in low-lying states of $(1+1)$-dimensional conformal field theories, J. High Energy Phys. 10 (2019) 181.
[32] J. Zhang and M. A. Rajabpour, Subsystem distances between quasiparticle excited states, J. High Energy Phys. 07 (2022) 119.
[33] M. Žnidarič, T. Prosen, and P. Prelovšek, Many-body localization in the Heisenberg XXZ magnet in a random field, Phys. Rev. B **77**, 064426 (2008).
[34] D. A. Huse, R. Nandkishore, and V. Oganesyan, Phenomenology of fully many-body-localized systems, Phys. Rev. B **90**, 174202 (2014).
[35] F. Haake, M. Kuś, and R. Scharf, Classical and quantum chaos for a kicked top, Z. Phys. B Condens. Matter. **65**, 381 (1987).
[36] X. Wang, S. Ghose, B. C. Sanders, and B. Hu, Entanglement as a signature of quantum chaos, Phys. Rev. E **70**, 016217 (2004).
[37] G. J. Milburn, Simulating nonlinear spin models in an ion trap, arXiv:quant-ph/9908037.
[38] S. Dogra, V. Madhok, and A. Lakshminarayan, Quantum signatures of chaos, thermalization, and tunneling in the exactly solvable few-body kicked top, Phys. Rev. E **99**, 062217 (2019).
[39] R. Alicki, D. Makowiec, and W. Miklaszewski, Quantum chaos in terms of entropy for a periodically kicked top, Phys. Rev. Lett. **77**, 838 (1996).
[40] S. Ghose, R. Stock, P. Jessen, R. Lal, and A. Silberfarb, Chaos, entanglement, and decoherence in the quantum kicked top, Phys. Rev. A **78**, 042318 (2008).
[41] S. S. Chehade and A. Vershynina, Quantum entropies, Scholarpedia **14**, 53131 (2019).
[42] M. Fannes, A continuity property of the entropy density for spin lattice systems, Commun. Math. Phys. **31**, 291 (1973).
[43] K. M. R. Audenaert, A sharp continuity estimate for the von Neumann entropy, J. Phys. A **40**, 8127 (2007).
[44] L. Vidmar and M. Rigol, Entanglement entropy of eigenstates of quantum chaotic Hamiltonians, Phys. Rev. Lett. **119**, 220603 (2017).
[45] L. Vidmar, L. Hackl, E. Bianchi, and M. Rigol, Entanglement entropy of eigenstates of quadratic fermionic Hamiltonians, Phys. Rev. Lett. **119**, 020601 (2017).
[46] T. LeBlond, K. Mallayya, L. Vidmar, and M. Rigol, Entanglement and matrix elements of observables in interacting integrable systems, Phys. Rev. E **100**, 062134 (2019).
[47] J. Šuntajs, J. Bonča, T. Prosen, and L. Vidmar, Quantum chaos challenges many-body localization, Phys. Rev. E **102**, 062144 (2020).
[48] D. A. Abanin, J. H. Bardarson, G. De Tomasi, S. Gopalakrishnan, V. Khemani, S. A. Parameswaran, F. Pollmann, A. C. Potter, M. Serbyn, and R. Vasseur, Distinguishing localization from chaos: Challenges in finite-size systems, Ann. Phys. (N.Y.) **427**, 168415 (2021).
[49] D. Sels and A. Polkovnikov, Dynamical obstruction to localization in a disordered spin chain, Phys. Rev. E **104**, 054105 (2021).
[50] W. De Roeck and F. Huveneers, Stability and instability towards delocalization in many-body localization systems, Phys. Rev. B **95**, 155129 (2017).